Article

Effects of Sodium Silicate on Flotation Separation of Sphalerite and Dolomite and Its Mechanism

Longqian Ni [1,2], Jinfang Lv [1,2,*], Lingyu Kong [1,2] and Longwei Qin [1,2]

[1] Faculty of Land Resource Engineering, Kunming University of Science and Technology, Kunming 650093, China; longqianni@163.com (L.N.); lykong2023@163.com (L.K.); 15720709286@163.com (L.Q.)

[2] National and Local Joint Engineering Research Center for Green Comprehensive Utilization of Tailings Resources from Metal Ores, Kunming 650093, China

* Correspondence: jflv2017@126.com

Abstract: Sphalerite often co-exists with dolomite, a carbonate mineral containing calcium and magnesium. In the flotation process of sphalerite, dolomite entering into the concentrate will have a considerable negative impact on the subsequent smelting. Therefore, the effects of sodium silicate on the flotation separation of sphalerite and dolomite and its mechanism were investigated in this study. It was found that alkaline conditions and the addition of sodium silicate were conducive to the flotation separation of sphalerite and dolomite. Under alkaline conditions, sodium silicate improved the hydrophobicity of sphalerite and the slurry turbidity. The yield stress and apparent viscosity were significantly reduced when dolomite was present in slurry. In addition, the surface electrical properties of dolomite shifted from positive to negative with an increase in the dosage of sodium silicate at pH 11, leading to electrostatic repulsion between sphalerite and dolomite. EDLVO results indicated that the total interaction energy between dolomite and sphalerite particles was repulsive when sodium silicate was present. This study provided a theoretical basis for the flotation separation of sphalerite and dolomite.

Keywords: sphalerite; dolomite; sodium silicate; flotation separation

1. Introduction

Among non-ferrous metals, the global consumption of zinc ranks third after aluminum and copper. With the continuous development of the social economy and the continuous improvement of consumption levels, the demand for zinc products in the world is increasing year by year. Therefore, the efficient development and utilization of zinc ore resources are of great significance to the development of the national economy [1]. Sphalerite is the main zinc-bearing mineral and often coexists with carbonate minerals containing calcium and magnesium. Due to the poor interaction between sphalerite and xanthate, the sphalerite usually needs to be activated by adding copper ions. Carbonate minerals containing calcium and magnesium are often found in the form of dolomite in sphalerite ores [2]. Dolomite is mainly gelatinous and metasomatic with sphalerite, and some particles are fine-grained and wrap inside sphalerite, which leads to difficulty in ore grinding and dissociation, serious gangue inclusion, and entering flotation concentrate with sphalerite [3]. When zinc concentrate is smelted by pyrometallurgy, the magnesium oxide content in the furnace material is required to be strictly controlled within 5% [4]. This is due to the fact that most magnesium-containing minerals are substances with high melting points, increasing the smelting energy consumption, and causing the slag to stick to the furnace wall. When hydrometallurgical is used, the content of magnesium-containing

silicate minerals is too high, resulting in an increase in the amount of sulfuric acid, and the accumulation of dissolved magnesium ions in the acid solution eventually clogs the filter cloth due to the precipitation of magnesium sulfate crystals. Therefore, there is an urgent need to develop a method to reduce the magnesium content during sphalerite flotation.

Currently, the method of separating sulfide minerals from calcium–magnesium minerals is mainly flotation. The gangue containing magnesium in sulfide ore mainly includes serpentine, talc, and dolomite. It is often necessary to add depressants or dispersants to the slurry to reduce the floatability of gangue minerals, thus preventing them from entering the concentrate [5–8]. Magnesium depressants can be divided into two categories: organic depressants and inorganic depressants. The depressant types of gangue containing magnesium are shown in Table 1. Organic depressants include polysaccharides, tannins, humic acids, and organic synthetic polymers [9]. Inorganic depressants include phosphates and silicates [10]. Polysaccharide organic depressants mainly include starch, dextrin, guar gum, xanthan gum, sweet potato gum, lignin, pectin, carrageenan, chitosan, and locust bean gum [11–14]. In addition, in order to improve the depressor effect of polysaccharide organic depressants, the predecessors have been modified, and the common ones are modified starch, carboxymethyl cellulose, and carboxylated chitosan [15]. The most commonly used dispersants are sodium hexametaphosphate, sodium tripolyphosphate, and sodium silicate [16,17]. Sodium hexametaphosphate can alleviate the heterogeneous condensation of magnesium-containing gangue and useful minerals and change the surface potential of magnesium-bearing gangue, enhancing the electrostatic repulsion between particles. The reaction mechanism of sodium hexametaphosphate is mainly through the formation of hydrophilic complexes, adsorption on the surface of minerals, changing their surface electrical properties, and dispersing and depressing them [18–20]. The dispersion mechanism of sodium silicate is mainly due to the reduction in mineral surface potential and the change in electrostatic force between mineral particles through $SiO(OH)_3{}^-$, so as to improve the dispersion effect between particles.

Table 1. Depressants of gangue containing magnesium.

Categories	Depressants	Other Reagents	Research Technique	Application	Ref.
Organic reagents	Starch	Acetic acid HCl/NaOH Dodecyl amine	Zeta potential XPS AFM	Lab	[21]
	Dextrin	HCl/NaOH NaBX Terpenic oil	Zeta potential Infrared spectroscopic Adsorption experiments	Lab	[22]
	Locust bean gum	PBX SHMP Pine oil	Zeta potential Turbidity tests	Lab	[23]
Inorganic reagents	Sodium hexametaphosphate	HCl/NaOH CMC MIBC	Zeta potential FTIR Absorption and ion release	Lab/Plant	[24]
	Sodium silicate	Zinc sulfate Kerosene Terpinol oil	FTIR Zeta potential ToF-SIMS	Lab/Plant	[25]

Sodium silicate is an inorganic colloid, which is a commonly used regulator in flotation, and it has a good depressor effect on gangue minerals such as quartz and silicate. When

fluorite, calcite, and scheelite float with fatty acids as collectors, sodium silicate can be used as a depressant of gangue minerals. When the amount of sodium silicate is large, it also has a depressor effect on sulfide ore [26]. The depressing of sodium silicate is caused by $HSiO_3^-$ and H_2SiO_3, which adsorb on the surface of the minerals, making them highly hydrophilic. In addition, the adsorption degree of $HSiO_3^-$ and H_2SiO_3 on the surface of minerals is different, and minerals with strong adsorption capacity will be depressed, while conversely, minerals with poor adsorption capacity will not be depressed [27,28]. Another possible depressing mechanism is the repulsion between hydrophilic negatively charged mineral particles and hydrophobic negatively charged bubbles caused by the addition of sodium silicate [29–31]. In addition, sodium silicate is also often used as a dispersant in flotation. It is employed to improve the froth stability and increase the grade of concentrate. Sodium silicate is very useful for the flotation of minerals with a large sludge content. However, adding too much sodium silicate can make concentrate filtration difficult. The mechanism of sodium silicate as a sludge dispersant is that the silicate colloids are negatively charged and have a hydration layer on their surface, and the silicate colloids are stably dispersed and suspended in the slurry without agglomeration and sedimentation with each other [32]. When this colloidal particle and $HSiO_3$ are adsorbed on the surface of the sludge, the sludge is in a dispersed state, which can play an important role in improving the froth performance in the beneficiation and desliming operation [33]. Although a large number of studies have been carried out on the role and mechanism of sodium silicate in flotation, it is unclear whether sodium silicate can improve the flotation effect of dolomite and sphalerite.

In the study, sphalerite and dolomite were taken as the research objects, and the effects of sodium silicate on the flotation behavior of sphalerite and dolomite were investigated by microbubble flotation tests. Turbidity tests were used to determine the dispersion of single minerals and artificially mixed minerals. The effects of sodium silicate on the surface wettability of dolomite and sphalerite were studied by contact angle measurement. The effects of sodium silicate on the rheological properties of slurry were clarified by rheological properties. The dynamic potential measurement was used to reveal the change rules of mineral electrical properties before and after reaction with sodium silicate. Through the theoretical calculation of EDLVO, the interaction force between particles before and after the reaction with the reagent was revealed. This study lays a theoretical foundation for the flotation separation of sphalerite and dolomite.

2. Materials and Methods

2.1. Samples and Reagents

Sphalerite and dolomite samples used in this study were sourced from Jiangxi Province and Yunnan Province, China. The samples were first crushed using crushers, followed by grinding with a three-head agate grinder. The milled sphalerite and dolomite were sieved with standard sieves to obtain sphalerite and dolomite particles with a size of -37 μm. Sphalerite and dolomite samples were analyzed by X-ray diffraction (XRD), and the results of the XRD analysis are charted in Figure 1. There were no characteristic peaks of other minerals in the samples of sphalerite and dolomite. Chemical element analysis indicated that the Zn grade in sphalerite was 64.23% and the purity of sphalerite reached about 95.85%. Dolomite contained 20.93% MgO and its purity was approximately 96.28%.

CaO and HCl (Aladdin Biochemical Co., Ltd., Shanghai, China) were used to adjust the pH of the slurry. Copper sulfate ($CuSO_4$, 99%, Maclin Biochemical Technology Co., Ltd., Shanghai, China) and sodium silicate (Na_2SiO_3, 97%, Shanghai Maclin Biochemical Technology Co., Ltd.) were used as the regulator. Butyl xanthate and terpineol oil (Tiefeng Mineral Processing Pharmaceutical Co., Ltd., Kunming, China) were employed as collectors

and the frother, respectively. The reagents used were analytically pure, and deionized water was used for all the experiments.
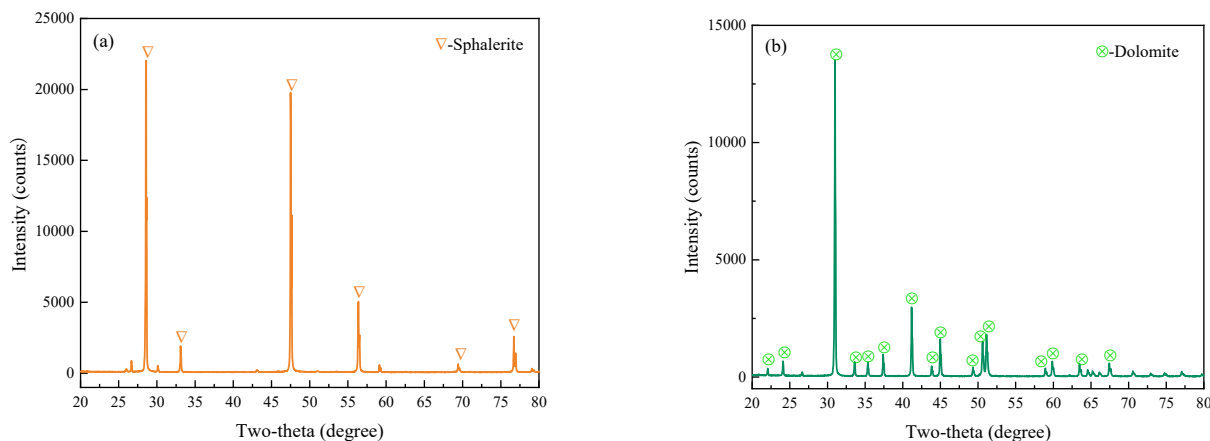
Figure 1. XRD pattern of sphalerite (**a**) and dolomite (**b**).

2.2. Flotation Tests

The flotation tests were conducted using a flotation machine (XFG-II, Exploration Machinery Plant, Jilin China), with a 40 mL effective-volume cell. First, the sphalerite and dolomite samples were mixed according to the weight ratio of 1:1, and 4 g of mixed samples was poured into the flotation tank with 35 mL of deionized water. The impeller speed of the flotation machine was set to 1993 r/min, and an airflow rate of 6 L/min was used. The pH of the slurry was adjusted with CaO and HCl, and then copper sulfate with a concentration of 1×10^{-4} mol/L, sodium silicate with a concentration in the range of 0–100 mg/L, and butyl xanthate with a concentration of 1×10^{-4} mol/L were added sequentially for 3 min. Then, pineol oil with a concentration of 5 mg/L was conditioned for 1 min, and the flotation time was fixed at 3 min. Finally, the obtained concentrate and tailings were filtered, dried, and weighed for tests. The average value was recorded by repeating tests three times.

2.3. Contact Angle Measurements

The contact angle is an important indicator of the wettability of the mineral surface [34]. The contact angle measurement was conducted by a contact-angle-measuring instrument (JA-200, IFEisi Precision Instrument Co., Ltd., Shanghai, China). Samples of sphalerite and dolomite with a volume of $1 \times 1 \times 0.3$ cm^3 were obtained by slicing. The sliced samples were polished with 1000-mesh sandpaper, after which the sanded samples were cleaned with deionized water. The contact angles were measured after reaction with the flotation reagents, and the average values were taken by repeating measurements 3 times.

2.4. Turbidity Experiments

Turbidity is used to characterize the dispersed state of mixed minerals [35]. A 0.5 g amount of dolomite was added to 40 mL of deionized water and stirred with a magnetic stirrer for 3 min. During the stirring, the slurry was adjusted to the required pH with CaO solution, 0.5 g of sphalerite was added, and after stirring for 3min, it was transferred to the settling tube. Deionized water in a 100 mL volume was added to the settling tube, and settled for 20 min after stirring. After that, 10 mL of supernatant was transferred to an LH-WGZ-1B turbidity meter. When the turbidity is large, it means that the number of mineral particles in the upper suspension of the sedimentation system is large, and the slurry is in a dispersed state. On the contrary, when the turbidity is small, it means that

the number of mineral particles in the upper suspension is small, and the slurry is in an aggregated state [36].

2.5. Slurry Rheology Measurements

Rheology measurement analyzes the relationship between stress and strain in the flow of fluids [37]. The rheology tests were performed using a rheometer (MCR702, Anton Paar GmbH, Graz, Austria). The pure mineral sample was stirred after adding reagents according to the requirements, then 40 mL of slurry was added to the test sample cup. The shear yield stress and apparent viscosity of the slurry were measured. Shear stress data and rheological characteristic data were obtained, and the average values were taken.

2.6. Zeta Potential Measurements

The potential was determined using sphalerite and dolomite samples with a particle size of -5 μm. A 20 mg sample was transferred to a beaker with 40 mL of deionized water. After stirring with a magnetic stirrer, the pH of the solution was adjusted with CaO solution for 3min. Then, the mixture was left to stand for 10 min. A 2.5 mL amount of supernatant was transferred to an electrophoresis tank, and measured by a Malvern Zetasizer Nano-ZS900pro instrument (Sibaiji Instrument System Co., Ltd., Shanghai, China) three times. The average value was taken.

2.7. EDLVO Theory Analysis

EDLVO theory [38,39] is an extension of the classical DLVO theory, which is often used to explain the interaction forces between particles. The formula of EDLVO theory is shown in Equation (1). The equations used to calculate the interaction between sphalerite and dolomite particles are listed in Table 2.

$$\mathrm{V}_T^{ED} = V_W + V_E + V_H \tag{1}$$

where V_T^{ED} is the total interaction energy; V_W is the Van der Waals interaction energy; V_E is the electrostatic interaction energy; and V_H is the hydrophobic interaction energy. When V_T^{ED} is positive, there is a repulsive force between the particles. When V_T^{ED} is negative, there is an attraction between the two particles.

Table 2. Formula for EDLVO calculation between sphalerite and dolomite particles [29,30].

Van der Waals interaction energy	$A_{132} = \left(\sqrt{A_{11}} - \sqrt{A_{33}}\right)\left(\sqrt{A_{22}} - \sqrt{A_{33}}\right)$ $V_W = -\frac{A_{132}}{6H}\frac{R_s R_d}{R_s + R_d}$	$A_{11} = 5.45 \times 10^{-20}$; $A_{22} = 4.87 \times 10^{-20}$; $A_{33} = 3.7 \times 10^{-20}$
Electrostatic interaction energy	$\kappa^{-1} = 0.304/\sqrt{C}$ $V_E = \frac{\pi \varepsilon_a R_s R_d}{R_s + R_d}\left(\varphi_{01}^2 + \varphi_{02}^2\right)\left\{\frac{2\varphi_{01}\varphi_{02}}{\varphi_{01}^2 + \varphi_{02}^2}\ln\left[\frac{1+\exp(-\kappa H)}{1-\exp(-\kappa H)}\right] + \ln[1-\exp(-2\kappa H)]\right\}.$	$C = 0.01$ mol/L; $\varepsilon_a = 6.95 \times 10^{-10}$ C^{2}J^{-1}m^{-1} $\varphi_{01} = -44.14 \times 10^{-3}$ $\varphi_{02} = -39.45 \times 10^{-3}$
Hydrophobic interaction energy	$(1 + \cos\theta)\gamma_L = 2\left(\sqrt{\gamma_s^d \gamma_L^d} + \sqrt{\gamma_s^- \gamma_L^+}\right)$ $V_H^0 = 2\left[\sqrt{r_3^+}\left(\sqrt{r_1^-} + \sqrt{r_2^-} - \sqrt{r_3^-}\right) + \sqrt{r_3^-}\left(\sqrt{r_1^+} + \sqrt{r_2^+} - \sqrt{r_3^+}\right) - \sqrt{r_1^+ r_2^-} - \sqrt{r_1^- r_2^+}\right].$ $V_H = 2\pi \frac{R_s R_d}{R_s + R_d} h_0 V_H^0 \exp\left(-\frac{H}{h_0}\right)$	$r_3^+ = r_3^- = 25.5$; $\gamma_1^+ = \gamma_2^+ = \gamma_3^+ = 0$ $h_0 = 1$

3. Results and Discussion

3.1. Micro-Flotation Experiments

The effects of slurry pH and dosage of sodium silicate on the flotation separation of sphalerite and dolomite were investigated, and the results are shown in Figures 2 and 3, respectively.
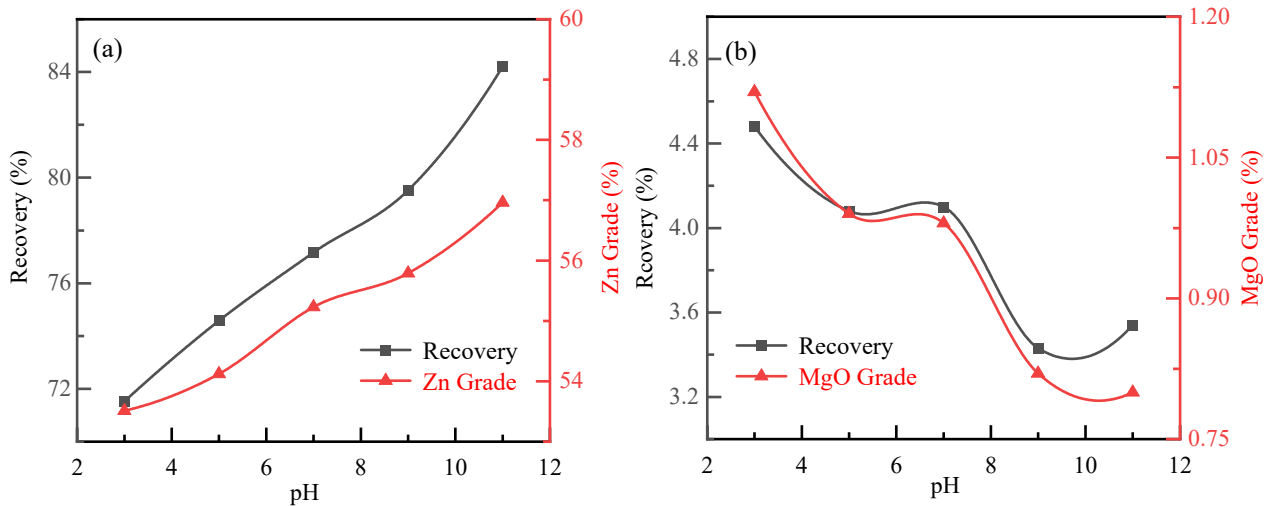
Figure 2. Effects of pH on flotation separation of sphalerite (**a**) and dolomite (**b**) in the flotation of mixed minerals (sodium silicate dosage of 20 mg/L).
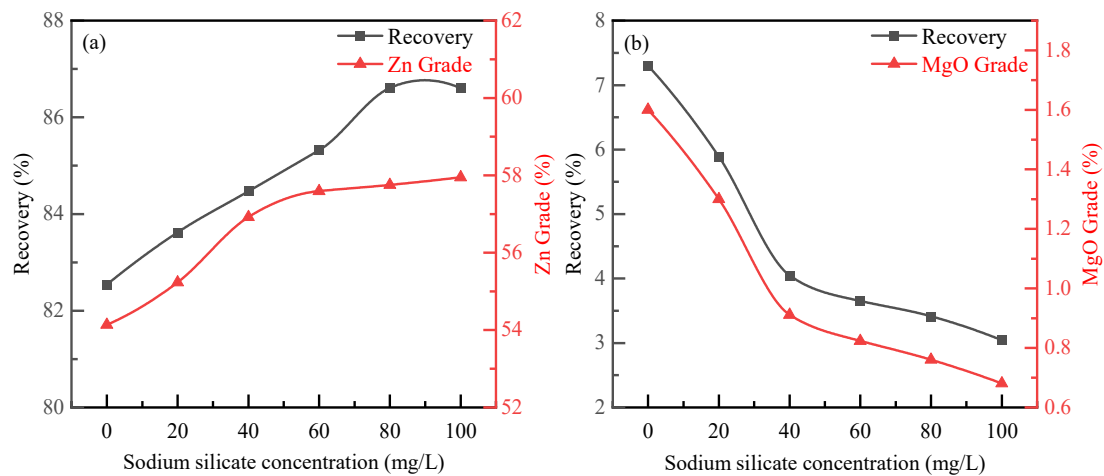
Figure 3. Effects of dosage of sodium silicate on flotation separation of sphalerite (**a**) and dolomite (**b**) in flotation of mixed minerals at pH 11.

Figure 2 exhibits the effects of slurry pH on the flotation separation of sphalerite and dolomite in mixed minerals under the condition of a sodium silicate dosage of 20 mg/L. As can be seen from the figure, the slurry pH demonstrated a great influence on the flotation separation of sphalerite and dolomite. Under acidic conditions, the flotation recovery of Zn was inferior. When the pH rose from 3 to 11, the flotation recovery of Zn increased from 71.52% to 84.20%, and the grade of Zn increased from 53.51% to 56.96%. This result showed that the increase in slurry pH was conducive to the improvement of Zn grade and recovery. In the flotation process, the flotation recovery of MgO showed a downward trend with an increase in pH, from 4.48% to 3.54%. Simultaneously, the MgO grade in the flotation concentrate was reduced from 1.12% to 0.80%. The flotation results indicated that the slurry pH exhibited a significant effect on the flotation separation of sphalerite and dolomite, and it was conducive to the flotation separation of sphalerite and dolomite under alkaline conditions.

When the pH value of the slurry was fixed at 11, the effects of the dosage of sodium silicate on the flotation separation of sphalerite and dolomite in mixed minerals were studied, and the results are presented in Figure 3. As can be seen from the figure, the flotation recovery and Zn grade increased with an increase in sodium silicate dosage. At a

sodium silicate dosage of 80 mg/L, the maximum recovery of Zn reached 86.61%, and the grade of Zn reached 57.75%. However, the flotation recovery and grade of MgO gradually decreased with the increase in the dosage of sodium silicate. When the sodium silicate dosage was in the range of 0 to 40 mg/L, the flotation recovery and grade of MgO decreased significantly. When sodium silicate was absent, the flotation recovery of MgO was 7.30%, and the MgO grade was 1.60%. When the sodium silicate concentration reached 100 mg/L, the flotation recovery and grade of MgO were minimized at 3.04% and 0.68%, respectively. The results implied that the addition of sodium silicate effectively reduced the flotation recovery of dolomite, and the floatability of sphalerite was improved, which promoted the flotation separation of sphalerite and dolomite.

3.2. Wettability Analysis

During the flotation, mineral wettability is usually measured by the contact angle. The larger the contact angle on the surface of minerals, the more hydrophobic and floatable the mineral [40]. Figure 4 illustrates the contact angles of sphalerite and dolomite before and after the addition of the sodium silicate at pH 11. This study indicated that in the absence of sodium silicate, the contact angle of the dolomite surface was 28.95° and that of the sphalerite surface was 42.3°. The results were consistent with previous studies [41,42]. When sodium silicate was present, the contact angles of dolomite and sphalerite were 20.08° and 55.38°, respectively. Compared with the absence of sodium silicate, the surface contact angle of dolomite was reduced, indicating that sodium silicate enhanced the hydrophilicity of dolomite. However, the surface contact angle of sphalerite was significantly increased, which indicated that the sodium silicate improved the hydrophobicity of sphalerite. The contact angle results were consistent with the previous flotation results.
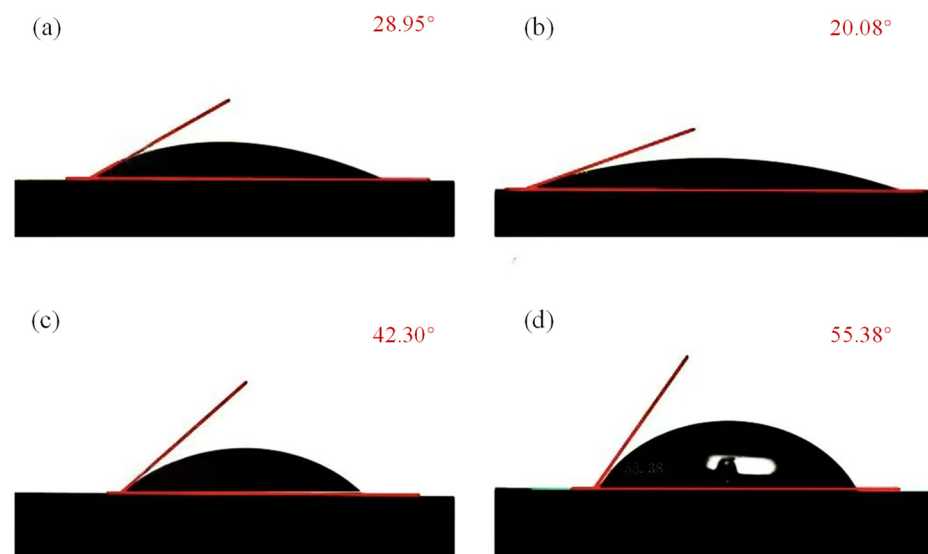
Figure 4. Contact angles of dolomite and sphalerite before and after reaction with sodium silicate: (**a**) dolomite + CaO, (**b**) dolomite+ CaO + Na_2SiO_3, (**c**) sphalerite + CaO, (**d**) sphalerite + CaO + Na_2SiO_3.

3.3. Turbidity Tests

The slurry turbidities of sphalerite, dolomite, and mixed minerals under different concentrations of sodium silicate were measured by a turbidity meter, and the results are demonstrated in Figure 5. In the absence of sodium silicate and at pH 11, the slurry turbidity of sphalerite was lower than that of dolomite, which indicated that the dispersion of dolomite in the slurry was better than that of sphalerite in the slurry. With the increase in the sodium silicate concentration, the turbidity of dolomite slurry showed a significant

upward trend, while the turbidity value of sphalerite slurry increased slowly, indicating that the concentration of sodium silicate exhibited a significant influence on the turbidity of dolomite slurry, and sodium silicate achieved an excellent dispersion effect for dolomite. When sphalerite and dolomite existed at the same time, the turbidity value showed an upward trend with an increase in sodium silicate concentration, indicating that sodium silicate can improve the dispersion of the slurry system and reduce the covering degree of dolomite on the sphalerite.
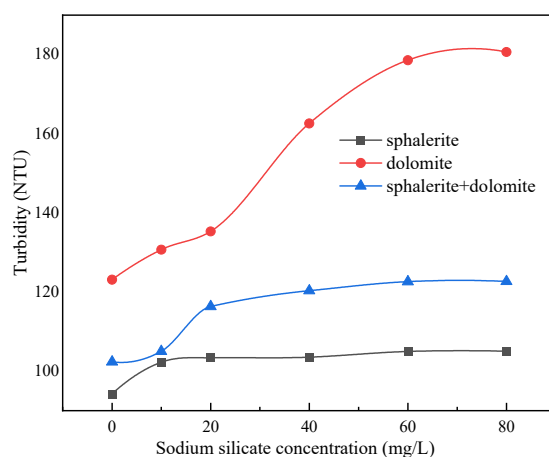
Figure 5. Effects of sodium silicate concentration on the turbidity of slurry of sphalerite and dolomite at pH 11.

3.4. Rheological Properties of Slurry

Rheological analysis can reveal the level of interparticle interaction and aggregation in the slurry, which is closely related to flotation performance. Shear yield stress and viscosity are the main parameters for evaluating the rheological properties of flotation pulp [43].

In order to study the effect of sodium silicate concentration on the rheology of slurry of sphalerite and dolomite, the yield stress and apparent viscosity of sphalerite and dolomite slurry under different sodium silicate concentrations were investigated at pH 11, and the results are shown in Figure 5. As can be seen from Figure 6a, the yield stress of dolomite slurry was higher than that of sphalerite slurry over the entire sodium silicate concentration range. With an increase in sodium silicate concentration, the yield stress of dolomite slurry decreased from 0.098 Pa to 0.024 Pa. Nevertheless, the yield stress of sphalerite slurry remained almost constant around 0.004 Pa. In addition, when both sphalerite and dolomite existed in the slurry, the yield stress of the slurry decreased with an increase in sodium silicate concentration, indicating that the addition of sodium silicate changed the rheological properties of the mixed slurry. Figure 6b shows the apparent viscosity of the slurry as a function of sodium silicate concentration. It was found that the viscosity of sphalerite slurry was almost not affected by sodium silicate concentration, and was lower than 11 mPa·s. However, with an increase in sodium silicate concentration, the apparent viscosity of dolomite decreased significantly, from 15.21 mPa·s to 10.21 mPa·s. In addition, the apparent viscosity of the slurry in the coexistence system of sphalerite and dolomite showed a downward trend, from 13.78 mPa·s to 10.12 mPa·s. The results indicated that the addition of sodium silicate reduced the yield stress and apparent viscosity of the mixed slurry, thereby increasing the flotation rate and selectivity of the flotation reagent during the flotation process [44,45]. Thus, the flotation separation effect between sphalerite and dolomite was improved.
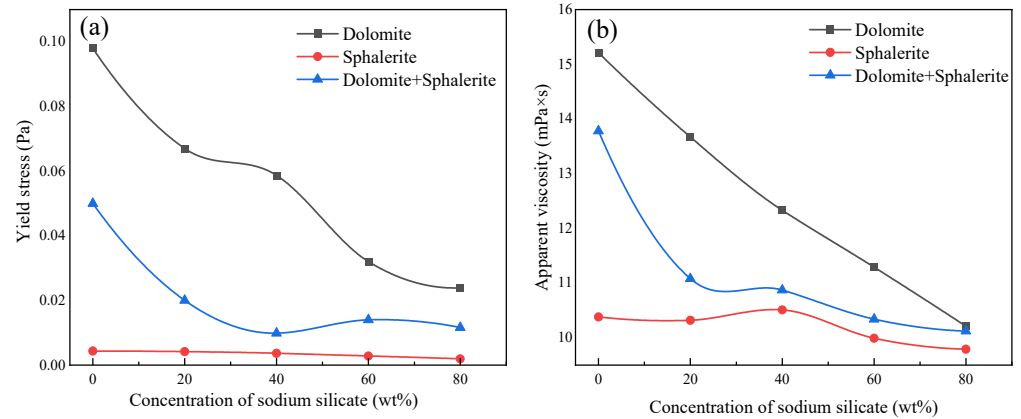
Figure 6. Effects of sodium silicate concentration on yield stress (**a**) and apparent viscosity (**b**) of sphalerite and dolomite slurry at pH 11.

3.5. Zeta Potential Analysis

The adsorption of flotation reagents often alters the electrostatic properties of the mineral surface. Figure 7 depicts the zeta potential of dolomite and sphalerite as a function of sodium silicate concentration at pH 11. In the absence of sodium silicate, the potential of dolomite was positive, while the potential of sphalerite was negative, leading to an electrostatic attraction between them. As the concentration of sodium silicate increased, the zeta potential on the surface of sphalerite and dolomite gradually decreased. When the concentration of sodium silicate was higher than 11 mg/L, the potential of dolomite and sphalerite were negative, resulting in them repelling each other and reducing the cover phenomenon of dolomite on the surface of sphalerite. These were consistent with the turbidity and flotation results.
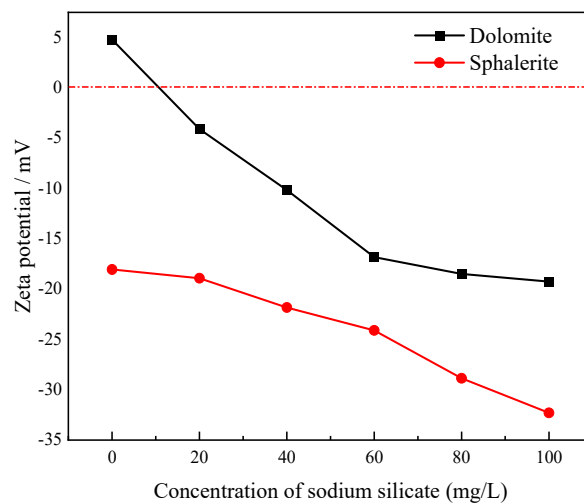
Figure 7. Effects of sodium silicate concentration on zeta potential of sphalerite and dolomite at pH 11.

3.6. EDLVO Theory

Figure 8 shows the interaction energies between dolomite and sphalerite particles before and after reaction with sodium silicate at pH 11. In the absence of sodium silicate, the Van der Waals energy, electrostatic energy, and hydrophobic energy between sphalerite and dolomite particles were negative, indicating that the forces between the particles were attractive. When sodium silicate was present, the electrostatic energy, hydrophobic energy, and total energy of dolomite and sphalerite became positive, indicating that a strong mutual

repulsion force between the two particles appeared, and the hydrophobic energy was the main force [46].
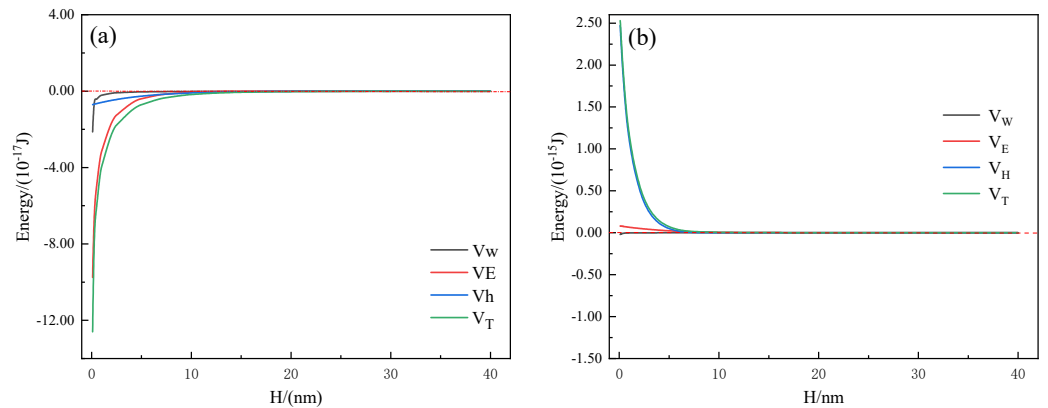
Figure 8. Interaction energy between sphalerite and dolomite particles before (**a**) and after (**b**) interaction with sodium silicate at pH 11.

3.7. Discussion

In the absence of sodium silicate, the zeta potentials on the surface of sphalerite and dolomite were negative and positive, respectively, resulting in electrostatic adsorption and inferior flotation separation. After treatment with sodium silicate, both sphalerite and dolomite exhibited negative zeta potentials, resulting in potential repulsion. In addition, sodium silicate enhanced the hydrophilicity of dolomite and the hydrophobicity of sphalerite, and the dispersion effect and rheological properties of pulp were improved. In the presence of sodium silicate, a strong mutual repulsion force between the two particles appeared. Therefore, sodium silicate effectively strengthened the flotation separation of sphalerite and dolomite. A schematic diagram is shown in Figure 9.
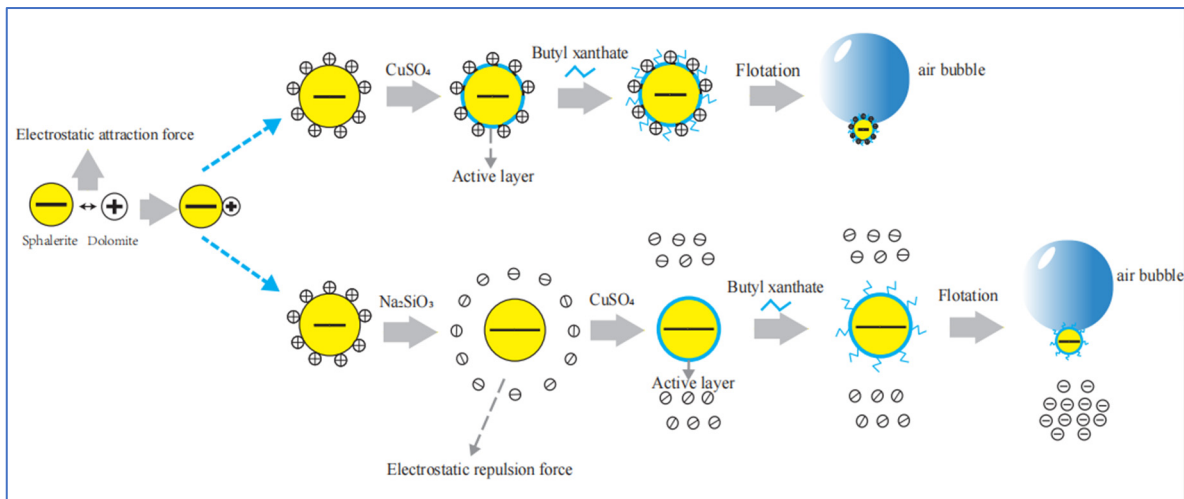
Figure 9. Schematic diagram of sodium silicate enhancing the separation of sphalerite and dolomite.

4. Conclusions

The effects of dolomite on sphalerite flotation and the enhanced separation mechanism of dolomite and sphalerite were investigated in this study. The conclusions are as follows:

(1)   Sodium silicate improved the grade and recovery of sphalerite, while it reduced the floatability of dolomite, enhancing the flotation separation of sphalerite and dolomite. The surface contact angle of dolomite decreased, while that of sphalerite increased

after reaction with sodium silicate. With an increase in sodium silicate dosage, the dispersion effect of slurry was improved.

(2) Sodium silicate improved the dispersion of the slurry system and reduced the covering degree of dolomite on the sphalerite. In addition, it reduced the yield stress and apparent viscosity of the mixed slurry.

(3) In the absence of sodium silicate, the zeta potentials on the sphalerite and dolomite surfaces were negative and positive, respectively, resulting in heterogeneous agglomeration. In both sphalerite and dolomite treated with sodium silicate, the zeta potentials turned negative, resulting in electrostatic repulsion.

(4) EDLVO theoretical calculations indicated that the cover between sphalerite and dolomite particles mainly depended on electrostatic interaction energy when sodium silicate was absent. In the presence of sodium silicate, a strong mutual repulsion force between the two particles appeared.

References

1. Nayak, A.; Jena, M.S.; Mandre, N.R. Beneficiation of Lead-Zinc Ores—A Review. *Miner. Process. Extr. Metall. Rev.* **2022**, *43*, 564–583. [CrossRef]

2. Jia, C.Y.; Wei, D.Z.; Li, P.J.; Li, X.J.; Tai, P.D.; Liu, W.; Gong, Z.Q. Selective adsorption of Mycobacterium Phlei on pyrite and sphalerite. *Colloids Surf. B Biointerfaces* **2011**, *83*, 214–219. [CrossRef] [PubMed]

3. Feng, B.; Lu, Y.-p.; Feng, Q.-M.; Ding, P.; Luo, N. Mechanisms of surface charge development of serpentine mineral. *Trans. Nonferrous Met. Soc. China* **2013**, *23*, 1123–1128. [CrossRef]

4. Yu, Z.; Liu, Z.; Ye, F.; Xia, L. Corrosion mechanism of magnesia-chrome and alumina-chrome refractories in E-scrap smelting. *Ceram. Int.* **2022**, *48*, 2693–2703. [CrossRef]

5. Cao, J.; Tian, X.-D.; Luo, Y.-C.; Hu, X.-Q.; Xu, P.-F. The effect of graphene oxide on the slime coatings of serpentine in the flotation of pentlandite. *Colloids Surf. A Physicochem. Eng. Asp.* **2017**, *522*, 621–627. [CrossRef]

6. Chen, Y.; Zhang, G.; Shi, Q.; Yang, S.; Liu, D. Utilization of tetrasodium iminodisuccinate to eliminate the adverse effect of serpentine on the flotation of pyrite. *Miner. Eng.* **2020**, *150*, 106235. [CrossRef]

7. Liu, C.; Zheng, Y.; Yang, S.; Fu, W.; Chen, X. Exploration of a novel depressant polyepoxysuccinic acid for the flotation separation of pentlandite from lizardite slimes. *Appl. Clay Sci.* **2021**, *202*, 105939. [CrossRef]

8. Tang, X.; Chen, Y. Using oxalic acid to eliminate the slime coatings of serpentine in pyrite flotation. *Miner. Eng.* **2020**, *149*, 106228. [CrossRef]

9. Yang, C.; Song, G.; Zhang, P.; Wang, C.; Gao, X.; Li, M. Exploration of a novel depressant pullulan gum for the flotation separation of specularite from aegirite. *Miner. Eng.* **2024**, *210*, 108666. [CrossRef]

10. Malysiak, V.; O'Connor, C.T.; Ralston, J. Pentlandite-feldspar interaction and its effect on separation by flotation. *Int. J. Miner. Process.* **2002**, *66*, 89–106. [CrossRef]

11. Khraisheh, M.; Holland, C.; Creany, C.; Harris, P.; Parolis, L. Effect of molecular weight and concentration on the adsorption of CMC onto talc at different ionic strengths. *Int. J. Miner. Process.* **2005**, *75*, 197–206. [CrossRef]

12. McFadzean, B.; Dicks, P.; Groenmeyer, G.; Harris, P.; O'Connor, C. The effect of molecular weight on the adsorption and efficacy of polysaccharide depressants. *Miner. Eng.* **2011**, *24*, 463–469. [CrossRef]

13. Morris, G.E.; Fornasiero, D.; Ralston, J. Polymer depressants at the talc–water interface: Adsorption isotherm, microflotation and electrokinetic studies. *Int. J. Miner. Process.* **2002**, *67*, 211–227. [CrossRef]

14. Shortridge, P.G.; Harris, P.J.; Bradshaw, D.J.; Koopal, L.K. The effect of chemical composition and molecular weight of polysaccharide depressants on the flotation of talc. *Int. J. Miner. Process.* **2000**, *59*, 215–224. [CrossRef]

15. Zhao, K.; Gu, G.; Wang, C.; Rao, X.; Wang, X.; Xiong, X. The effect of a new polysaccharide on the depression of talc and the flotation of a nickel–copper sulfide ore. *Miner. Eng.* **2015**, *77*, 99–106. [CrossRef]

16. Ramirez, A.; Rojas, A.; Gutierrez, L.; Laskowski, J.S. Sodium hexametaphosphate and sodium silicate as dispersants to reduce the negative effect of kaolinite on the flotation of chalcopyrite in seawater. *Miner. Eng.* **2018**, *125*, 10–14. [CrossRef]

17. Li, W.; Li, Y. Improved understanding of chalcopyrite flotation in seawater using sodium hexametaphosphate. *Miner. Eng.* **2019**, *134*, 269–274. [CrossRef]

18. Bai, J.; Wang, J.; Yin, W.; Chen, X. Influence of Sodium Phosphate Salts with Different Chain Length on the Flotation Behavior of Magnesite and Dolomite. *Minerals* **2020**, *10*, 1031. [CrossRef]

19. Dho, H.; Iwasaki, I. Role of sodium silicate in phosphate flotation. *Min. Metall. Explor.* **1990**, *7*, 215–221. [CrossRef]

20. Zhao, K.; Yan, W.; Wang, X.; Wang, Z.; Gao, Z.; Wang, C.; He, W. Effect of a novel phosphate on the flotation of serpentine-containing copper-nickel sulfide ore. *Miner. Eng.* **2020**, *150*, 106276. [CrossRef]

21. Yang, S.; Xu, Y.; Kang, H.; Li, K.; Li, C. Investigation into starch adsorption on hematite and quartz in flotation: Role of starch molecular structure. *Appl. Surf. Sci.* **2023**, *623*, 157064. [CrossRef]

22. Dong, J.; Liu, Q.; Subhonqulov, S.H. Effect of dextrin on flotation separation and surface properties of chalcopyrite and arsenopyrite. *Water Sci. Technol.* **2020**, *83*, 152–161. [CrossRef] [PubMed]

23. Feng, B.; Zhang, W.; Guo, Y.; Peng, J.; Ning, X.; Wang, H. Synergistic effect of acidified water glass and locust bean gum in the flotation of a refractory copper sulfide ore. *J. Clean. Prod.* **2018**, *202*, 1077–1084. [CrossRef]

24. Lu, J.; Sun, M.; Yuan, Z.; Qi, S.; Tong, Z.; Li, L.; Meng, Q. Innovative insight for sodium hexametaphosphate interaction with serpentine. *Colloids Surf. A Physicochem. Eng. Asp.* **2019**, *560*, 35–41. [CrossRef]

25. Wu, W.; Chen, T.; Shao, Y.; Ye, G.; Tong, X. The flotation separation of molybdenite from talc using zinc sulfate in sodium silicate system and related mechanism. *Colloids Surf. A Physicochem. Eng. Asp.* **2022**, *641*, 128451. [CrossRef]

26. Long, T.; Zhao, H.; Wang, Y.; Yang, W.; Deng, S.; Xiao, W.; Lan, X.; Wang, Q. Synergistic mechanism of acidified water glass and carboxymethyl cellulose in flotation of nickel sulfide ore. *Miner. Eng.* **2022**, *181*, 107547. [CrossRef]

27. Liu, M.; Hu, B.; Zhang, C.; Wang, Q.; Sun, Z.; He, P.; Chen, Y.; Chen, D.; Zhu, J. Effect of sodium silicate on the flotation separation of chalcopyrite and galena using sodium sulfite and sulfonated lignin as depressant. *Miner. Eng.* **2022**, *182*, 107563. [CrossRef]

28. Jin, J.; Gao, H.; Chen, X.; Peng, Y. The separation of kyanite from quartz by flotation at acidic pH. *Miner. Eng.* **2016**, *92*, 221–228. [CrossRef]

29. Gomez-Flores, A.; Park, H.; Hong, G.; Nam, H.; Gomez-Flores, J.; Kang, S.; Heyes, G.W.; Leal Filho, L.d.S.; Kim, H.; Lee, J.M.; et al. Flotation separation of lithium–ion battery electrodes predicted by a long short-term memory network using data from physicochemical kinetic simulations and experiments. *J. Ind. Inf. Integr.* **2024**, *42*, 100697. [CrossRef]

30. Yoon, R.-H.; Mao, L. Application of Extended DLVO Theory, IV: Derivation of Flotation Rate Equation from First Principles. *J. Colloid. Interface Sci.* **1996**, *181*, 613–626. [CrossRef]

31. Gomez-Flores, A.; Solongo, S.K.; Heyes, G.W.; Ilyas, S.; Kim, H. Bubble−particle interactions with hydrodynamics, XDLVO theory, and surface roughness for flotation in an agitated tank using CFD simulations. *Miner. Eng.* **2020**, *152*, 106368. [CrossRef]

32. Ramirez, A.; Gutierrez, L.; Laskowski, J.S. Use of "oily bubbles" and dispersants in flotation of molybdenite in fresh and seawater. *Miner. Eng.* **2020**, *148*, 106197. [CrossRef]

33. Hao, H.; Li, L.; Yuan, Z.; Liu, J. Comparative effects of sodium silicate and citric acid on the dispersion and flotation of carbonate-bearing iron ore. *J. Mol. Liq.* **2018**, *271*, 16–23. [CrossRef]

34. Brookes, G.F.; Bethell, P.J. Zeta potential, contact angle and the use of amines in the chemical dewatering of froth-floated coal. *Powder Technol.* **1984**, *40*, 207–214. [CrossRef]

35. Zhang, X.-G.; Zhang, J.; Ye, W.-l.; Pan, C.-L.; Wei, X.-X.; Hu, X.-Q.; Luo, Y.-C.; Xu, P.-F. Studies on the application of N,N-bis(phosphonomethyl)-sulfamic acid in the selective flotation separation of pyrite from serpentine. *Miner. Eng.* **2022**, *183*, 107602. [CrossRef]

36. Wang, X.; Yuan, S.; Liu, J.; Zhu, Y.; Han, Y. Nanobubble-enhanced flotation of ultrafine molybdenite and the associated mechanism. *J. Mol. Liq.* **2022**, *346*, 118312. [CrossRef]

37. Spaull, A.J.B. An Introduction to Rheology By H. A. Barnes, J. F. Hutton and K. Walters, Elsevier Science Publishers, Amsterdam, 1989. 200 pp, price US$92.00/Dfl. 175.00 (Hardcover), US$60.50/Dfl. 115.00 (Paperback). ISBN 0 444 87140 3 (Hardcover), ISBN 0–444–87469-0 (Paperback). *J. Chem. Technol. Biotechnol.* **1991**, *50*, 437. [CrossRef]

38. Li, D.; Yin, W.; Liu, Q.; Cao, S.; Sun, Q.; Zhao, C.; Yao, J. Interactions between fine and coarse hematite particles in aqueous suspension and their implications for flotation. *Miner. Eng.* **2017**, *114*, 74–81. [CrossRef]

39. Li, Q.; Liao, C.; Hou, J.; Wang, W.; Zhang, J. A mathematic model based on eDLVO and Lifshitz theory calculating interparticle interactions in coal water slurry. *Fuel* **2022**, *316*, 123271. [CrossRef]

40. Ma, X.; Nguyen, N.N.; Nguyen, A.V.; Miller, J.D. An investigation of mineral floatability versus mineral surface exposure and hydrophobicity by high-resolution X-ray microcomputed tomography, film flotation, contact angles, and modeling. *Miner. Eng.* **2023**, *200*, 108139. [CrossRef]

41. Wang, C.; Liu, R.; Xie, F.; Zhai, Q.; Sun, W.; Wen, X.; Li, J. Separation of sphalerite and dolomite using sodium alginate as an environmentally friendly depressant in a carbonate-hosted Pb-Zn ore system. *J. Clean. Prod.* **2022**, *380*, 135107. [CrossRef]

42. Subrahmanyam, T.V.; Prestidge, C.A.; Ralston, J. Contact angle and surface analysis studies of sphalerite particles. *Miner. Eng.* **1996**, *9*, 727–741. [CrossRef]

43. Liu, D.; Zhang, G.; Gao, Y. New perceptions into the detrimental influences of serpentine on Cu-Ni sulfide flotation through rheology studies and improved the separation by applying garnet. *Miner. Eng.* **2021**, *171*, 107110. [CrossRef]

44. Liu, D.; Zhang, G.; Chen, Y.; Chen, W.; Gao, Y. A Novel Method to Limit the Adverse Effect of Fine Serpentine on the Flotation of Pyrite. *Minerals* **2018**, *8*, 582. [CrossRef]

45. Gao, Y.; Zhang, G.; Wang, M.; Liu, D. The Critical Role of Pulp Density on Flotation Separation of Nickel-Copper Sulfide from Fine Serpentine. *Minerals* **2018**, *8*, 317. [CrossRef]

46. Zhou, H.; Xu, L.; Wang, D.; Xue, K.; Tian, J. Selective adsorption mechanism of SHMP onto fine fluorite in bastnaesite flotation system. *Colloids Surf. A Physicochem. Eng. Asp.* **2023**, *670*, 131527. [CrossRef]